Cu-Albumin Artificial Enzymes with Peroxidase and Oxidase Activity for Stereoselective Oxidations

Maham Liaqat,¹ Emma McDonald,¹ Robert Jervine Valdez Ortega,¹ Aaron Lopes,^{2,3} Flavia Codreanu,^{2,4} Hannah Carlisle,^{2,5} Challa V. Kumar,^{1,6} Xudong Yao,^{1,6} James F. Rusling,^{1,6,7,8} and Jie He^{1,6*}

Keywords: Artificial enzymes; Biocatalysis; Copper phthalocyanine; Bovine serum albumin; Epoxidation; Artificial peroxidase; Chiral oxidation.

ABSTRACT: We herein report a design of artificial enzymes by incorporating a synthetic copper complex into non-catalytic bovine serum albumin (Cu-BSA) to carry out stereoselective oxidation. This Cu-BSA catalyst with stably bound Cu complex as a co-factor shows peroxidase-like activity to catalyze epoxidation of styrene with high chiral selectivity (>99%) to R-styrene epoxide. With electrochemical conversion of Cu²⁺ to Cu⁺, Cu-BSA also exhibits oxidase-like activity to selectively reduce oxygen to hydrogen peroxide (H₂O₂), which can be combined with its peroxidase function to drive oxidation of C=C bonds using air. This artificial enzymatic system holds promise for chiral-selective transformations of non-natural substances and highlights the versatility of non-catalytic proteins in artificial enzyme design.

¹Department of Chemistry, University of Connecticut, Storrs, CT, 06269, USA

²Division of Gastroenterology, Department of Medicine, Brigham and Women's Hospital, Harvard Medical School, Boston, MA, 02115, USA

³Koch Institute for Integrative Cancer Research, Massachusetts Institute of Technology, Cambridge, MA, 02139, USA

⁴Department of Chemistry, University of Toronto, Toronto, ON, M5S 3H6, Canada

⁵Department of Chemistry, Northeastern University, Boston, MA, 02115 USA

⁶Institute of Materials Science, University of Connecticut, Storrs, CT, 06269, USA

⁷Department of Surgery and Neag Cancer Center, UConn Health, Farmington, CT, 06030, USA

⁸School of Chemistry, National University of Ireland at Galway, Galway, H91 TK33, Ireland

1. Introduction

Metalloenzymes are biological catalysts that use metal ions as cofactors to drive chemical reactions.^{1, 2} Examples include iron-heme-enzymes, such as cytochrome P450s (cyt P450s) and peroxidases that are among the best oxidation catalysts for C-H bond activation.³⁻⁷ Cyt P450s particularly are involved in metabolism of about 75% of existing drugs and are of significant interest to chemists designing synthetic chiral oxidations. ^{4, 5, 8, 9} While metalloenzymes excel in their biocatalyst functions, they are not optimized to catalyze chemical transformations of non-natural substrates. 10, 11 Directed evolution of enzymes, by which enzymes are genetically engineered to improve desirable functions, has been demonstrated to enhance kinetics and introduce new functionalities beyond their native functions. ¹²⁻¹⁸ In a recent study by Yang et al., ¹⁷ a serine-ligated variant of Bacillus megaterium P450 (CYP102A1) was used to catalyze the radical addition step of atom transfer radical addition (ATRA) through dehalogenation. Although native CYP102A1 can catalyze intramolecular ATRA non-stereoselectively, engineered enzymes showed an improved enantioselectivity of >90% for a number of non-natural lactams. Despite being highly regio- and stereoselective, extensive use of natural metalloenzymes or engineered enzymes is still limited. Most enzymes are expensive and time-consuming to isolate and purify. 19 While cyt P450s can be used in partially purified lipid constructs such as supersomes and bacteriosomes, ¹⁷ these are still quite expansive for scaleup applications. In addition, the use of coenzymes in many enzymatic reactions also increases the cost substantially. Cyt P450s, as an example, need coenzymes like nicotinamide adenine dinucleotide phosphate (NAPDH) and cytochrome P450 reductase (CPR) as electron and proton donors to activate oxygen.

There have been extensive efforts to design artificial enzymes that combine a synthetic metal cofactor in a protein scaffold where the protein binding pocket provides a well-defined geometry to host catalytic metal site(s) and specific affinity to activate reactions. Among these, apoenzymes equipped with non-natural metal cofactors can significantly improve activity over natural metalloenzymes and simultaneously retain stereoselectivity. Early studies from Yamamura *et al.* demonstrated that the Zn^{2+} co-factor of carboxypeptidase A could be replaced with a redox active Cu^{2+} co-factor and Cu^{2+} carboxypeptidase A showed typical oxidase activity, *e.g.*, oxidation of ascorbate with k_{cat} of 6 min⁻¹. Additionally, artificial enzymes can also be designed from inexpensive, non-catalytic natural proteins into which synthetic metal complexes are incorporated as active sites. For example, amphiphilic β -pyrroles can bind noncovalently with

human serum albumin (HSA).^{33, 34} While HSA is not catalytically active, it provides a chiral environment to drive the stereoselective oxidization catalyzed by bound co-factor, Fe- and Mn-containing β-pyrroles. Those hybrid catalysts were stereoselective for the oxidation of aryl methyl sulfides with an enantiomeric excess up to 70%. In a similar context, bovine serum albumin (BSA), a serum albumin protein derived from cows, also possesses multiple binding sites capable of binding hydrophilic and hydrophobic metal complexes.^{35, 36} Water soluble amphiphilic tetrasulfonate phthalocyanine–copper complex can interact with BSA to catalyze the Diels–Alder reaction of azachalcones with cyclopentadiene. The enantiomeric excess of those cycloaddition is up to 93%.³⁶ While incorporating soluble synthetic metal complexes within albumins can produce active "enzymes", those artificial enzymes are not as selective as metalloenzymes. A possible mechanism is the presence of weakly bound metal complexes at their secondary binding sites, mostly on the surface of the protein, where the catalytic microenvironment becomes heterogeneous.³³ In conventional wisdom, hydrophobic metal complexes are not possible to be included in the design of those artificial enzymes, because they have limited solubility in water and form aggregates.

We herein report a new design of artificial enzymes using non-catalytic serum albumins, into which hydrophobic, insoluble copper tetraaza-29H,31H-phthalocyanine (CuTPC) complex is incorporated as a catalytic site. The hydrophobic nature of CuTPC limits its weak interaction with albumins and provides an intact, single protein-ligand complex. Despite its low solubility, the balance of $CuTPC(s) \rightleftharpoons CuTPC(aq) \rightleftharpoons BSA-CuTPC(aq)$ allows the encapsulation of CuTPC in BSA by simply stirring a large excess of particulate CuTPC with an aqueous solution of BSA overtime to form 1:1 adducts as Cu-BSA. CuTPC bound to BSA shows typical circular dichroism (CD) spectroscopic features, indicating a specific and identical binding site for all Cu complexes. The bound CuTPC acts as a cofactor of Cu-BSA, to drive oxidase- and peroxidase-like activities. We show that Cu-BSA, upon activation by H₂O₂, can catalyze stereoselective epoxidation of styrene with >99% chiral selectivity to R-styrene epoxide. This high stereoselectivity arises from the chiral environment of BSA, whereas the denaturation of proteins would decrease stereoselectivity. Using electrochemically accessible Cu²⁺-to-Cu⁺ conversion, Cu-BSA also reduces oxygen selectively to hydrogen peroxide (H₂O₂) with a selectivity of 82-98% at a potential window of -0.55 V to -1.2 V vs. saturated calomel electrode (SCE). The oxygenase- and peroxidase-like activities of Cu-BSA can also be coupled to drive epoxidation of styrene using oxygen directly in which immobilized Cu-BSA on an electrode catalyzes the conversion of oxygen to peroxide, and dissolved Cu-BSA

in an electrolyte drives the epoxidation of styrene. Our approach to combine non-enzymatic proteins with hydrophobic synthetic metal complexes, therefore, provides a cost-effective way to design artificial enzymes for chiral-selective conversion of non-natural substances.

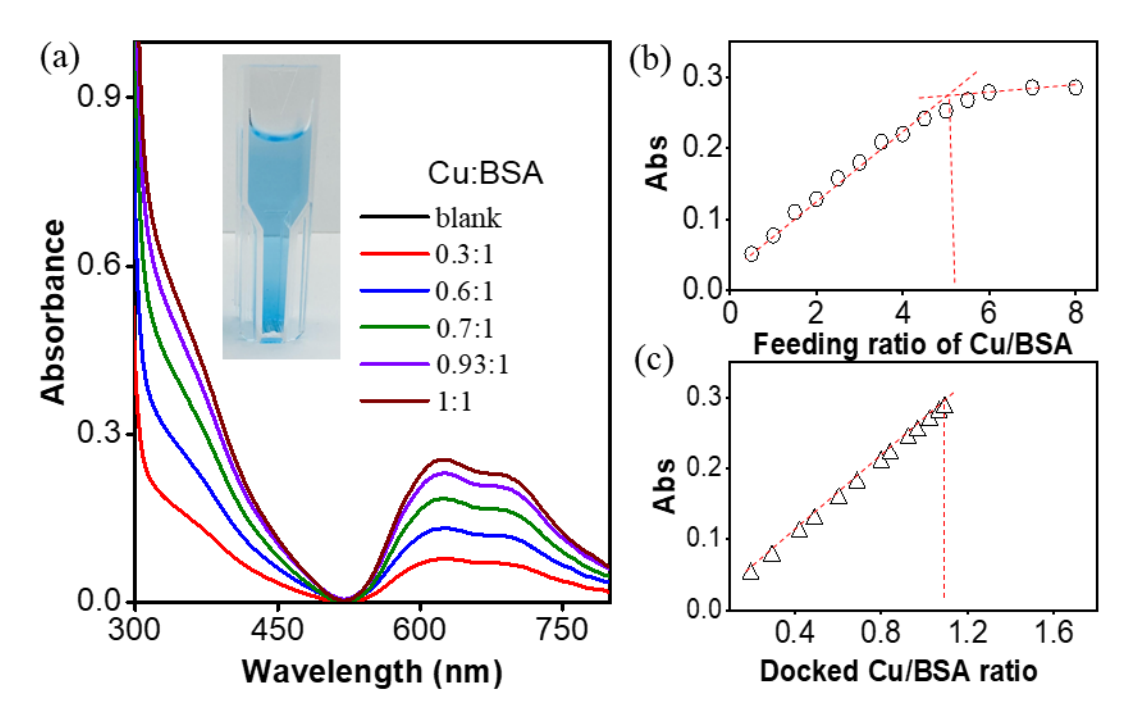


Figure 1. Formation of Cu-BSA complexes: (a) UV-vis at different feeding; (b,c) plotting feeding ratio of Cu/BSA (b) and docked Cu per BSA (c) using the absorbance at 622 nm.

2. Methods and Materials

2.1 Materials

CuTPC, horseradish peroxidase (HRP, 25,000 units), styrene, (S)-(-)-styrene oxide (enantiomer excess: 98%), (R) (+)-styrene oxide (enantiomer excess: 97%), and microemulsion components (see below) were purchased from Sigma-Aldrich and used as received. Bovine serum albumin (BSA) BAH66 Fatty Acid Free from Heat Shock was obtained from Equitech-bio, Inc. Bi-oMag®Plus carboxyl magnetic nanoparticles (1 μm diameter, 20 mg particles/mL) were procured from Polysciences, Inc. A water/oil bicontinuous microemulsion of cetyltrimethylammonium bromide (CTAB) was prepared with CTAB, 1-pentanol, tetradecane, and water (17.5:35:12.5:35, wt%) in accordance with previously published literature.³⁷

2.2 Characterization

The UV-vis spectra were recorded using a Cary 60 UV-Vis spectrophotometer, and the fluorescence spectra were measured on a Varian Cary Eclipse fluorescence spectrophotometer. The circular dichroism (CD) spectra were obtained using a Jasco J-710 CD spectrometer with a 0.05 cm path length quartz cuvette. The electron paramagnetic resonance (EPR) spectroscopy was performed using a Bruker EMX CW microspectrometer at room temperature. The electrochemical experiments were conducted using a single-compartment 3-electrode cell with a CH Instrument 660 electrochemical system. Platinum wire served as the counter electrode, and a saturated calomel electrode (SCE) was used as the reference electrode. The details on oxygen reduction and electrochemical synthesis are described in supporting information.

2.3 Coordination of CuTPC with BSA

We dispersed CuTPC with BSA in water at different molar ratios. The mixture was stirred over two days at room temperature. The solution was separated to remove insoluble CuTPC complex through centrifugation (10,000 rpm for 30 min). To determine the optimal binding of CuTPC with BSA, we examined the UV spectra at different loadings ranging from 1:1 to 8:1 (Cu: BSA, mol). Before centrifugation, there was a broad peak at ~800 nm, from insoluble CuTPC. We quantified the amount of CuTPC from 0 to 66 μM in acetic acid buffer at pH 4. We established the linear range of CuTPC to determine the stoichiometry of CuTPC-to-BSA. We calculated the Cu to BSA docking ratio using the Beer-Lambert law (Figure S1c). CuTPC has fluorescence in water, with a maximum emission peak at 685 nm as depicted in Figure S2a.

2.4 Peroxidase activity and analysis

The peroxidase-like activity was assessed using styrene epoxidation. Styrene was converted to styrene epoxide with H_2O_2 as an oxidant. The reaction was typically done by adding Cu-BSA (40 μ M) to a CTAB microemulsion solution containing H_2O_2 (8 mM) and styrene (4 mM) under mixing. The reaction was then incubated at 50°C for 120 min.

Before performing gas chromatography-mass spectrometry (GC-MS) and gas chromatograph-flame ionization detection (GC-FID) analysis, the reaction mixtures were purified using solid phase extraction on a silica column to remove surfactants. Styrene epoxide was confirmed

through GC-MS on an Agilent 7820 A GC system with a 5975 MSD series and a 12 m×200 μ m×0.33 μ m Restek column. To quantify the products, standards of R- and S-styrene epoxide were used to calibrate the GC. For GC analysis, 1 μ L of the solution was injected into the GC-MS system. The oven was operated using argon as the carrier gas, starting at 50 °C for 2 min, then ramping up to 240 °C at a rate of 10 °C/min, and finally running for 5 minutes at the highest oven temperature of 325 °C. From the mass spectrum, it was confirmed styrene epoxide as the only product.

For chiral GC chromatogram, the initial oven temperature was set at 100 °C for 8 min, followed by an increase to 180 °C at a rate of 4.0 °C/min over 20 min, resulting in a total run time of 28 min. Throughout the analyses, the injection and detector temperatures were consistently maintained at 220 °C and 250 °C, respectively. Chiral gas chromatography separation was performed using an HP 5890 gas chromatograph equipped with a flame ionization detector and a J&W Chiral CYCLODEX-B column with dimensions of 30 m, 0.25 mm, and 0.25 µm. Ultra-high purity nitrogen was used as the carrier gas, and ultra-high purity hydrogen and air were used to produce flames for the GC-FID. The calibration curves of styrene and styrene epoxide were also prepared with the internal standard, anisole. By plotting the peak intensities in relative to internal standard anisole, the molar concentration of substrates and products was determined using the relative peak areas in chromatograms.

3. Results and Discussion

BSA is a transport protein with discrete binding sites for various hydrophobic substances, including iron-heme, $^{38, 39}$ and other molecules. $^{40-42}$ Unlike water-soluble metal complexes, $^{33, 34, 43}$ the key challenge is the heterogenous protein-ligand binding due to the limited solubility. Our synthesis simply uses the strong shearing activation of CuTPC to continuously promote the solubilization and the formation of Cu-BSA complexes. 44 Excess CuTPC was first mixed with BSA at molar ratio of 5.5:1 (see SI for details). After stirring at room temperature for 48 h, CuTPC was slowly solubilized through non-covalent interactions with BSA. With a large excess of particulate CuTPC in the mixture, the equilibrium processes of CuTPC(s) \rightleftharpoons CuTPC(aq) \rightleftharpoons BSA-CuTPC(aq) likely promotes the binding of CuTPC to BSA. The shearing activation has previously proven to be effective even for graphite exfoliation. 44 This mixture was centrifuged to remove undissolved

CuTPC and the supernatant was collected as a light blue solution. UV-Vis spectroscopy reveals two absorption peaks at 622 and 695 nm, assigning to the Q band of CuTPC (Figure 1a). Our synthetic method can also be extended to other phthalocyanine complexes similarly. To confirm the optimal feeding ratio, we varied the concentration of CuTPC from 1:1 to 8:1 (mol, relative to BSA). The peak intensity of the Q band increased with the feeding ratio of CuTPC almost linearly and saturated at 5.5:1 (mol, Figure 1b). Using the standard curve of CuTPC in acetic buffer (pH 4, see Figure S1b), the binding ratio of CuTPC to BSA calculated from a Job's plot (Figure 1c), to be ~1.1, suggesting that BSA has a discrete binding pocket for CuTPC. This is different from the amphiphilic metal complexes with multiple binding sites (strong and weak binding models), simply because of the limited solubility of phthalocyanine complexes in water.

The formation of Cu-BSA was studied by mass spectroscopy (Figure 2a) and electron paramagnetic resonance (EPR) spectroscopy (Figure S2). Pristine BSA had an average molecular weight of 66.5 kDa, in good agreement with the reported value.³⁵ For Cu-BSA, the mass spectrum reveals two sets of peaks across the charge distribution. The most prominent peaks are from intact BSA protein. The Cu-BSA complex has a m/z 8.5 higher than that of BSA, a difference that correlates with CuTPC hosted in BSA. Docking analysis confirmed that CuTPC is located in between site-I (more inclined towards domain-II A and domain-I B, Figures 2c and S3) and site-II (domain III A). CuTPC has proximity to Ser-192 of 2.79 A° and His-145 of 3.85 A° of site-I. Using fluorescence emission from CuTPC, we titrated Cu-BSA with warfarin and ibuprofen as probes whose primary binding site to BSA are known and referred to as site-I and site-II, respectively (Figure S3). There was a fast decrease of fluorescence intensity by titration with warfarin (see Figure S4 for details), while no changes were observed with the titration of ibuprofen. Those results confirm that CuTPC most likely leans towards site-I, in consistence with the docking result.⁴⁶

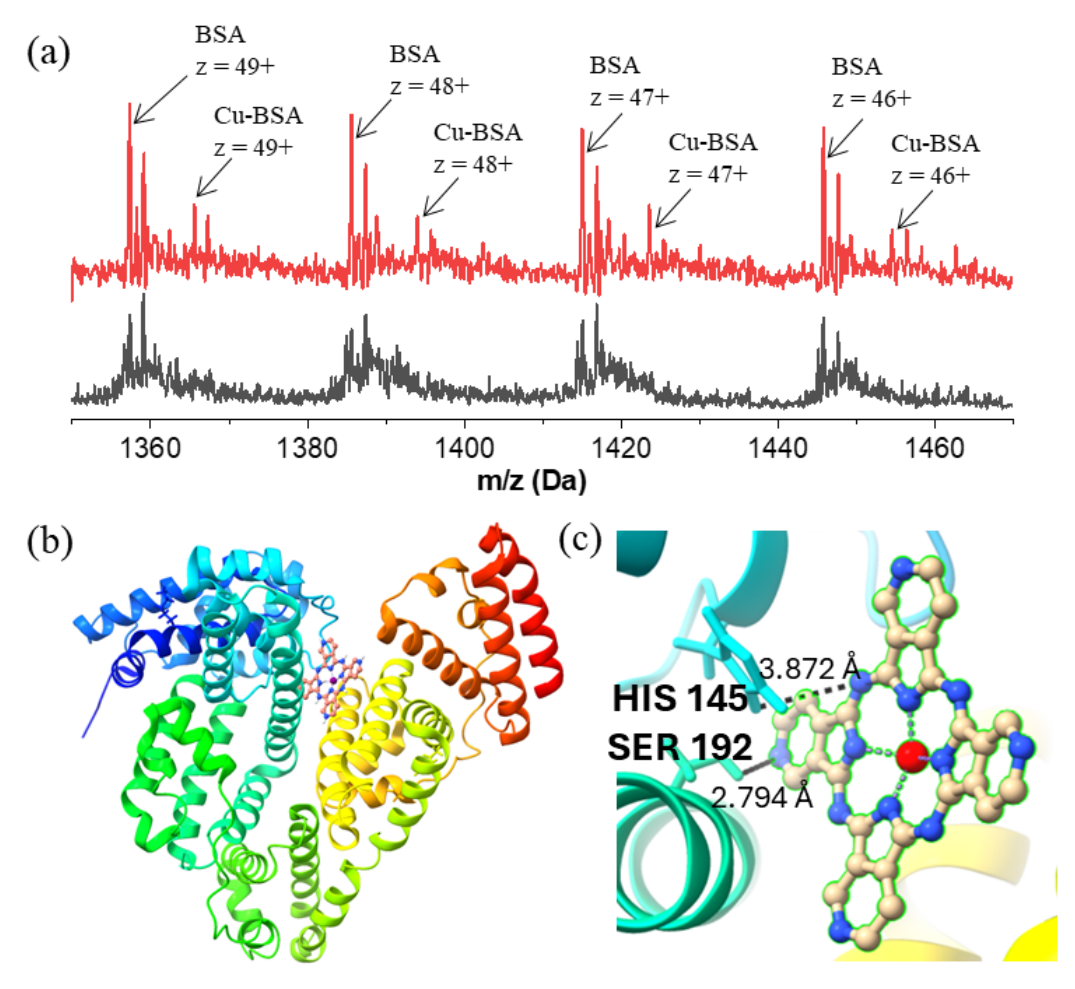


Figure 2. Formation of Cu-BSA complexes: (a) MS spectra of BSA (black, bottom) and Cu-BSA (red, top). (b-c) Docking analysis of Cu-BSA.

Figure 3a shows the circular dichroism (CD) spectra of BSA and Cu-BSA in the range of 200-300 nm. Overlapping of the two curves indicates an identical secondary structure of BSA and Cu-BSA. The structural integrity of BSA was also confirmed by agarose gel electrophoresis at pH 8 (Figure S5). After loading with CuTPC, negatively charged Cu-BSA shows only one sharp band very close to that of BSA. On the other hand, Cu-BSA has distinct induced CD bands in the visible region (Figure 3b). CD peak of Cu-BSA also increased linearly with the feeding ratio of CuTPC before saturation. The ellipticity saturated after all BSA was bound with Cu-BSA (Figure 3c). These CD spectra indicate that CuTPC is strongly bound with BSA in a chiral environment, similar to co-factors in natural metalloproteins. At pH 7, the Zeta potential of BSA is 29.4 mV and that

of Cu-BSA is 25.1 mV (Figure 3d), respectively. Both BSA and Cu-BSA have an isoelectric point at pH 4.7, confirming structural integrity of BSA as do the CD results.

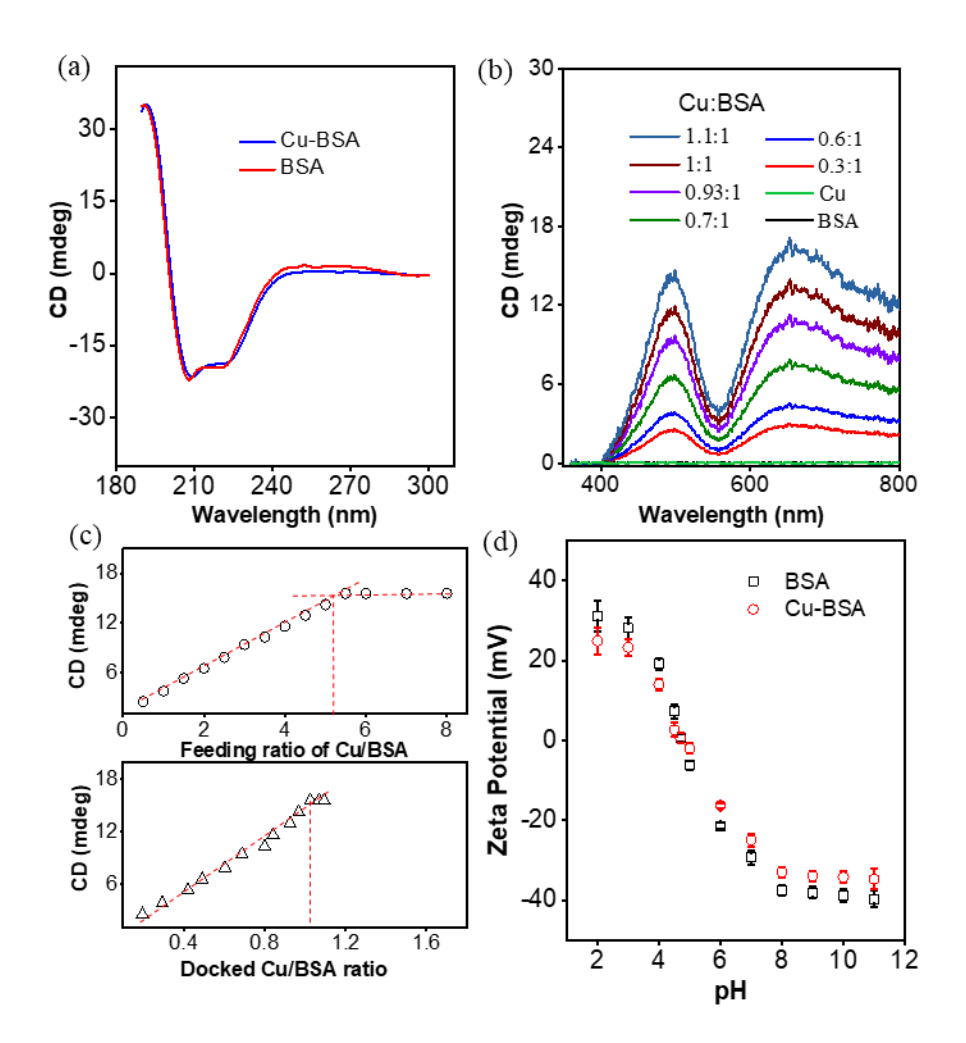


Figure 3. Secondary structure of BSA with/without CuTPC: (a-b) CD of BSA and Cu-BSA at different feeding and docking ratios of CuTPC in BSA; (c) ellipticity at different ratios of Cu/BSA; and (d) Zeta potential of BSA and Cu-BSA.

We examined peroxidase activity of Cu-BSA. Using styrene epoxidation as a model (Figure 4), the reaction was carried out in a bicontinuous microemulsion of cetyltrimethylammonium bromide (CTAB and see SI for details) to provides solubility to styrene.^{37, 48} In a typical reaction, 8 mM of H_2O_2 and 4 mM of styrene were mixed with 40 μ M of Cu-BSA at 50 °C. Styrene epoxide is the only product as confirmed by GC-MS (Figure S6). The chirality of reaction products was analyzed by gas chromatography (GC) using a chiral column (JW Chiral CYCLODEX-B), with

anisole as an internal standard. A racemic standard mixture of styrene epoxide (R/S) gave two well-separated peaks at 12.7 and 12.9 min (Figure 4), assigning to R- and S-styrene epoxide, respectively. After 2 h, the conversion to styrene oxide reached ~100% with chiral selectivity >99% to the R enantiomer. The reaction kinetics was samples at an interval of 20 min. Regardless of the styrene conversion, R-styrene epoxide is the only product (Figure 5a).

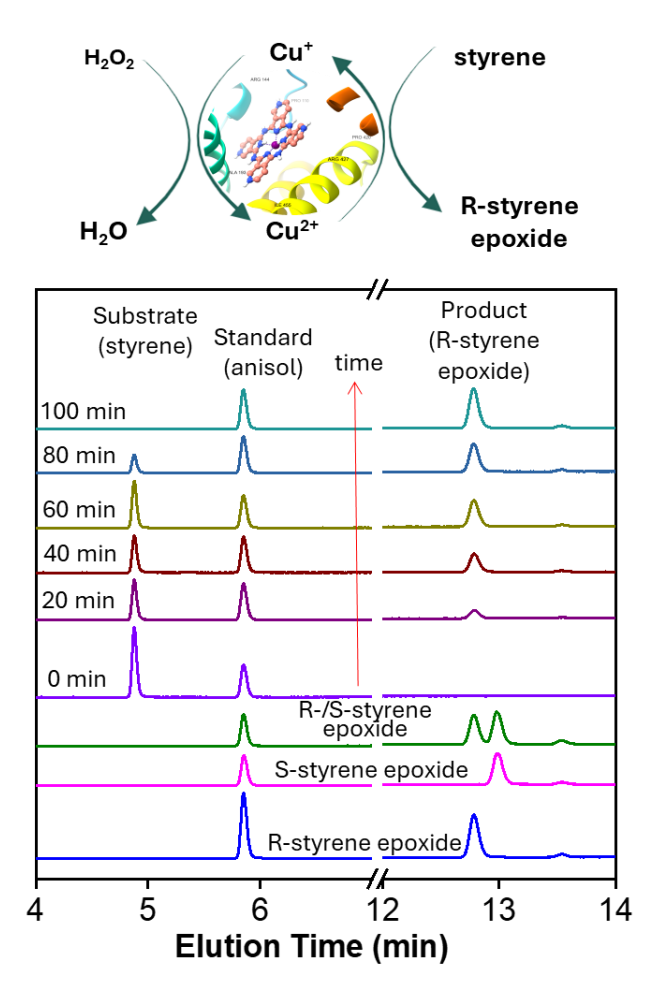


Figure 4. Styrene epoxidation catalyzed by Cu-BSA in CTAB microemulsion at 50 °C. Chiral GC elution curves of standards (bottom), reaction mixtures collected every 20 min interval.

The reaction fits well as first-order with a rate constant (k) of 0.03 min⁻¹ (Figure 5b). Enzymatic kinetics was also used to analyze through Michaelis-Menten model where the initial rate was measured for the first 35 min by quenching the reaction on silica gel column (Figure 5c). The initial rate was fitted using the product concentration (R-styrene epoxide) vs. reaction time. Figure 5d shows the fitting of the rate against the concentration of styrene. There is a quick saturation of

the rate against the concentration of styrene suggesting a high catalytic efficiency of Cu-BSA (also see Table S1). The turnover number k_{cat} of Cu-BSA was 4.2×10^{-2} s⁻¹. ^{49, 50} This activity is about four orders of magnitude greater than reported for horseradish peroxide (HRP) for styrene epoxidation in water. ⁵¹ We note that, styrene monooxygenases (SMOs) are the most prominent biocatalysts for styrene epoxidation with k_{cat} of 0.27-60 s⁻¹ as reported previously; however, their stere-oselectivity is only for S-styrene epoxide (>99% ee, Table S1). ⁵² Recently, the first natural SMO to synthesis R-styrene epoxide (91% ee) was identified from the genome of Streptomyces sp. NRRL S-31. ⁵³ Other monooxygenases, ^{49-51, 54-58} including cyt P450s, have been reported with catalytic selectivity to R-styrene epoxide (Table S1). However, those enzymatic cycles require the use of co-enzymes including nicotinamide adenine dinucleotide phosphate (NAPDH) and cyto-chrome P450 reductase (CPR) as electron donors. Thus, our design by combining inexpensive proteins with insoluble synthetic metal complexes as an artificial peroxidase is unique and valuable to achieve high R-enantioselectivity only with H₂O₂.

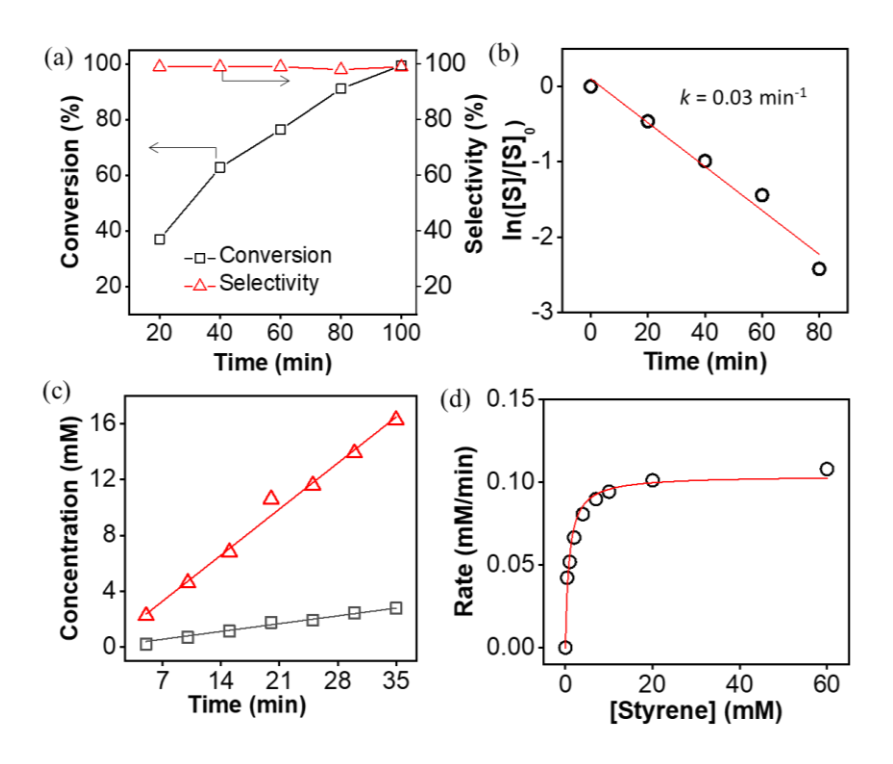


Figure 5. (a) Styrene conversion and selectivity of R-styrene epoxide vs. reaction time. (b) First-order reaction kinetics of Cu-BSA. (c) Initial rate measurement at styrene concentration of 0.4 mM (black) and 60 mM (red). (d) Michaelis-Menten plot on styrene epoxidation.

Control experiments confirmed the reaction selectivity. First, self-oxidation of styrene using H₂O₂ in absence of BSA and CuTPC led to racemic mixture of the epoxide (Run 13/14 in Table 1). In absence of BSA, CuTPC is catalytically active where 60% of styrene conversion was seen with a selectivity of R isomer, ~68% (Figure S6c). Second, no stereoselectivity was seen with denatured BSA. BSA lost its secondary structure at 80 °C (Figure S7). Denatured Cu-BSA had a conversion of 6.8% and a selectivity of R isomer, ~67% (Run 2), comparable to that of pure CuTPC. Similar results were observed with denatured BSA without CuTPC. With BSA, the selfoxidation of styrene had a conversion of 6% but its stereoselectivity is up to 98% (Table 1). The stereoselectivity is, therefore, a result of the chiral environment provided for CuTPC by BSA. We also note that, Cu-BSA as metal-protein complexes provides a key difference between studies to use BSA as a water-soluble ligand in organic synthesis.⁵⁹ The high stereoselectivity even at 100% conversion benefits largely from the identical chiral microenvironment of individual Cu site. The Cu-catalyzed epoxidation utilizing H₂O₂ can undergo a reactive •OH radical intermediate by cycling Cu²⁺/Cu⁺ 60 or, in some cases, Cu³⁺-O• intermediate. 61 Since the stereoselectivity was also observed in self-oxidation of styrene with pristine BSA, the catalytic epoxidation is likely mediated by •OH radicals with styrene bound to BSA. The molecular docking analysis confirmed that styrene favors docking at site I_A close to Ala 525 (Figure S8), in proximity to CuTPC where the catalytic decomposition of H₂O₂ occurs.

Table 1. Summarization of styrene epoxidation under various conditions. ^d

No.	Catalysts	[St]/[BSA]	H_2O_2	T	Conversion	Selectivity
		(mol)	(mM)	(°C)	(%)	to R* (%)
1	Cu-BSA	100:1	8 mM	50	99	99
2	Cu-BSA ^a	100:1	8 mM	50	6.8	67
3	Cu-BSA	100:1	8 mM	10	30	76
4	Cu-BSA	100:1	8 mM	20	59	86
5	Cu-BSA	100:1	8 mM	30	66	94
6	Cu-BSA	100:1	8 mM	40	78	99
7	Cu-BSA	100:1	8 mM	60	80	96
8	Cu-BSA	100:1	8 mM	70	60	84
9	Cu-BSA	100:1	0 mM	50	0	-
10	Cu-BSA, HRP ^b	25:1	96.5 μM	50	92	99
11	Cu-BSA, Cu-BSA b	25:1	96.5 μM	50	99	99
12	BSA	100:1	8 mM	50	6	98

13	-	catalyst-free	8 mM	50	5.7	58
14	CuTPC ^c	25:1	8 mM	50	60	68
15	BSA^a	100:1	8 mM	50	5	57

Note: ^a BSA is denatured at 80 °C. ^b Reactions carried out under electrochemically produced H₂O₂. ^c CuTPC dissolved at pH 4. ^d Reaction time: 2 h.

Enantioselectivity of Cu-BSA catalysis shows an interesting temperature-dependence. While reactivity decreased with temperature in a typical Arrhenius-behavior, there was a clear drop in selectivity for the R isomer. At 10 °C, the conversion was only 30% with enantioselectivity of 76% for R-styrene epoxide. Such temperature-dependent selectivity may be caused by decrease in conformational flexibility of the protein where the accessibility and binding of substrates could be limited, as reported previously. 62, 63 Increasing reaction temperature would improve the catalytic activity and selectivity simultaneously. At 50 °C, reaction was completed in 2 h with >99% enantioselectivity. Further increase in temperature disrupts the secondary structure of BSA, decreasing selectivity (Table 1).

The Cu sites hosted in BSA can further be immobilized on electrodes and they are electrochemically accessible as metalloenzymes. Cu-BSA can electro-catalyze oxygen reduction to H₂O₂ by oxygenase-like activity (Figure 6a). To examine electrocatalytic activity, negatively charged Cu-BSA was assembled on a pyrolytic graphite electrode with a positive polycation poly(diallyldimethyl ammonium chloride) in an layer-by-layer (LbL) film.³⁷ Figure 6a shows cyclic voltammetry (CV) of Cu-BSA in N₂ saturated PBS buffer at 50 mV/s. A pair of reversible peaks were seen at -0.62 V (cathodic) vs. SCE, assigning to reduction of Cu²⁺ to Cu⁺.64,65 After saturation with O₂, a cathodic catalytic peak for O₂ reduction was found at -0.59 V. The control bare electrode shows almost no reduction peak for O2. The oxygen reduction reaction (ORR) kinetics were investigated using ring disk voltammetry (RDV, Figures S9-10) and rotating ring-disk voltammetry (RRDV, Figure 6b). The number of electrons transferred (n) is close to 2 at potentials from -0.6 to -0.8 V. The yield of H₂O₂ measured by RRDV is 82-98% at potentials of -0.55 V to -1.2 V. Figure 6d shows constant-potential electrolysis at -0.6 V in the absence of styrene. The steady state current of Cu-BSA to produce H₂O₂ is very stable.H₂O₂ concentration was also measured using a colorimetric leuco crystal violet assay (see SI and Figure S11d). 66 Figure 6c shows that the concentration of H₂O₂ increased linearly with electrolysis time to 96.5 µM after 1 h at -0.6 V in PBS. The Faradaic efficiency (FE) to produce H₂O₂ was >85%.

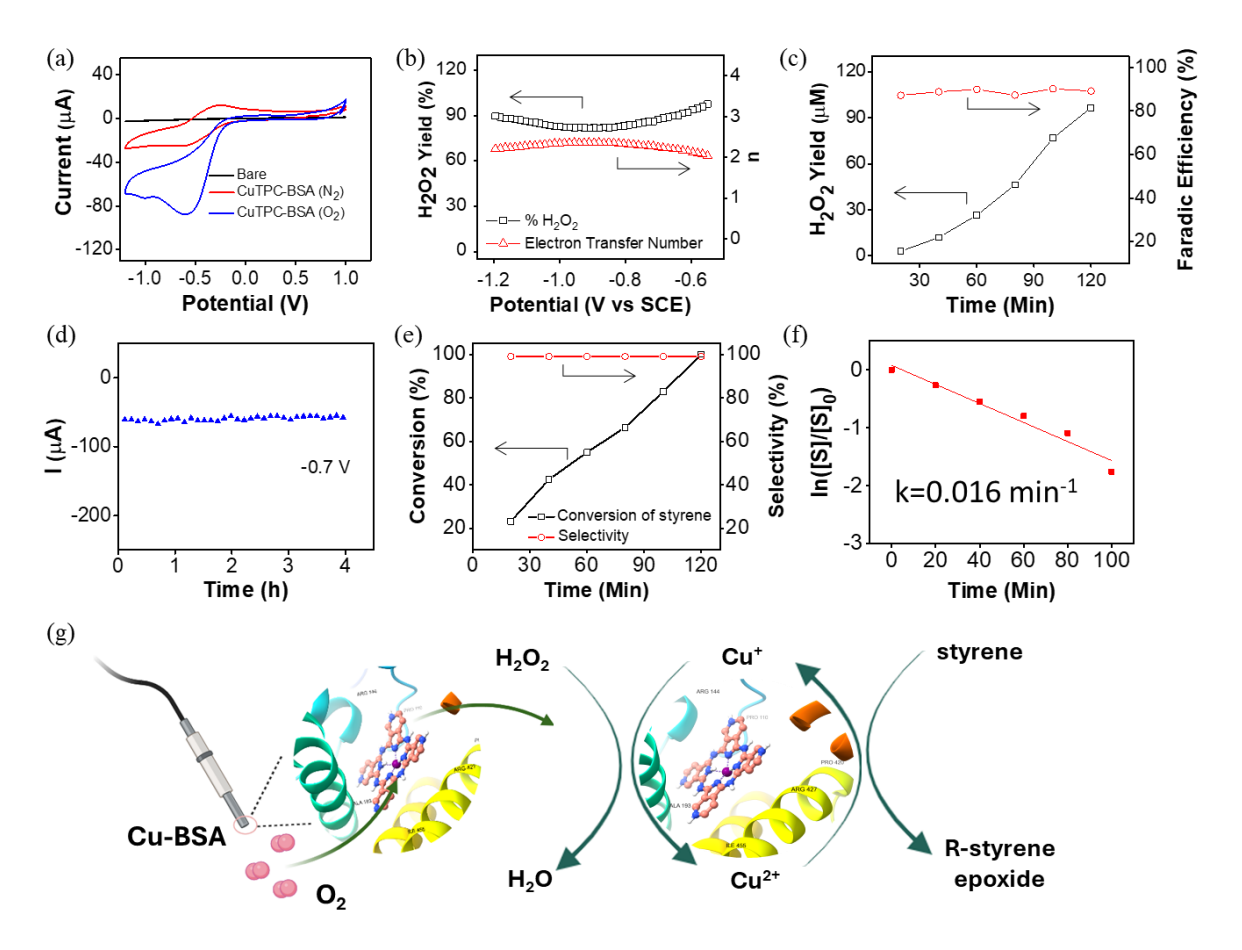


Figure 6. Oxidase activity of Cu-BSA. (a) Reaction scheme. (b) CVs of bare electrode (in O₂ saturated, black), and Cu-BSA at 50 mV/s in the N₂ (red) and O₂ (blue) saturated 0.1 M PBS buffer (pH 7). (c) Number of electron transfer and H₂O₂ efficiency of Cu-BSA measured from RRDV. (d) i-t curve of Cu-BSA for H₂O₂ production at -0.6 V. (e) H₂O₂ yield and FE of Cu-BSA towards H₂O₂ at -0.6 V using a colorimetry assay. (f,g) Plotting conversion/selectivity and kinetics through the cascade reaction of Cu-BSA.

We further combined the oxygenase- and peroxidase-like activities of Cu-BSA to drive epoxidation of styrene using oxygen directly (Figure 6g). A working electrode with Cu-BSA assembled on a screen-printed electrode (1×1 cm²) (see the setup in SI). Peroxidation was done in the CTAB microemulsion containing free Cu-BSA, with activation by H₂O₂ ORR product. After adding styrene, electrosynthesis of H₂O₂ was further coupled with the peroxidase-like Cu-BSA enzymes dispersed in the microemulsion. Using chiral CG, this coupled oxidation system had enantioselectivity of >99% to R-styrene epoxide with a yield as high as 92% after electrolysis for 2

h (Figure 6e). Figure 6f shows the first-order kinetic analysis. The rate constant was estimated to be 0.016 min⁻¹, about half of chemical epoxidation rate driven by H₂O₂. The rate is likely limited by the formation rate of H₂O₂, since the ratio of enzyme-to-substrate dispersed in microemulsion is higher to that in Figure 4. As a control, we measured the catalytic conversion by coupling Cu-BSA (as oxygenase) with HRP (as peroxidase) (Figures S11-S12 and Run 10 in Table 1). The two systems showed very similar efficiency.

4. Conclusion

In summary, the use of BSA as a cost-effective, non-catalytic protein scaffold in conjunction with synthetic CuTPC presents a promising approach for the development of artificial enzymes. Spectroscopic results suggested that CuTPC forms 1:1 adducts with BSA without disrupting the secondary structures of the protein. In the presence of H₂O₂, Cu-BSA catalyzed styrene epoxidation with >99% enantioselectivity to R-styrene epoxide. The k_{cat} of Cu-BSA reached 4.2×10⁻² s⁻¹, comparable to other natural peroxidases. Structural integrity and dynamics of the protein framework was found to be critical for the stereoselectivity of Cu-BSA. Denaturation of BSA would be detrimental to the selectivity of Cu-BSA. In addition to peroxidase-like activity, Cu-BSA also acted as an oxidase to activate molecular oxygen through electrocatalytic cycles of Cu⁺/Cu²⁺. At -0.6 V, Cu-BSA reduced oxygen to produce H₂O₂ with a selectivity >85%. The dual functionality of Cu-BSA was coupled for in situ reduction of oxygen to H₂O₂ and further use of H₂O₂ to drive epoxidation of styrene in a one-pot reaction. These findings demonstrate the versatility of Cu-BSA as an artificial enzyme with reactivity to catalyze oxygen activation and stereoselective epoxidation with high efficiency. This artificial enzyme system capitalizes on the affordability and broad availability of BSA, offering a valuable and inexpensive method for chiral-selective oxidation using either oxygen or H₂O₂ as an oxidant. This new approach will be useful for other noncatalytic natural proteins and synthetic metal complexes with high potential for low-cost green syntheses.

SUPPORTING INFORMATION

Oxygen reduction, chromatography methods, electrocatalytic synthesis, and more spectroscopic results. The Supporting Information is available free of charge at https://pubs.acs.org/.

ACKNOWLEDGEMENTS

J.H. and J.R. are grateful for the support from the National Science Foundation (CBET-2035669) and the University of Connecticut through the research excellence program.

AUTHOR INFORMATION

Corresponding Author

*Jie He, jie.he@uconn.edu

REFERENCES

- 1. Rehder, D., Bioinorganic chemistry. Oxford University Press Oxford: 2014.
- 2. Gonzalez-Granda, S.; Albarran-Velo, J.; Lavandera, I.; Gotor-Fernández, V., Expanding the synthetic toolbox through metal—enzyme cascade reactions. *Chem Rev* **2023**, *123* (9), 5297-5346.
- 3. Venkataraman, H.; Verkade-Vreeker, M. C. A.; Capoferri, L.; Geerke, D. P.; Vermeulen, N. P. E.; Commandeur, J. N. M., Application of engineered cytochrome P450 mutants as biocatalysts for the synthesis of benzylic and aromatic metabolites of fenamic acid NSAIDs. *Bioorgan Med Chem* **2014**, *22* (20), 5613-5620.
- 4. Guengerich, F. P., Mechanisms of cytochrome P450-catalyzed oxidations. *Acs Catal* **2018**, *8* (12), 10964-10976.
- 5. Kumar, N.; He, J.; Rusling, J. F., Electrochemical transformations catalyzed by cytochrome P450s and peroxidases. *Chem Soc Rev* **2023**, *52* (15), 5135-5171.
- 6. Liu, Z.; Huang, J.; Gu, Y.; Clark, D. S.; Mukhopadhyay, A.; Keasling, J. D.; Hartwig, J. F., Assembly and Evolution of Artificial Metalloenzymes within E. coli Nissle 1917 for Enantioselective and Site-Selective Functionalization of C— H and C= C Bonds. *J Am Chem Soc* **2022**, *144* (2), 883-890.
- 7. Bernhardt, R., Cytochromes P450 as versatile biocatalysts. J Biotech 2006, 124 (1), 128-145.
- 8. Krishnan, S.; Schenkman, J. B.; Rusling, J. F., Bioelectronic delivery of electrons to cytochrome P450 enzymes. *J. Phys. Chem. B* **2011**, *115* (26), 8371-8380.
- 9. Rusling, J. F.; Hvastkovs, E. G.; Schenkman, J. B., Drug Metabolism Handbook. *Nassar, A* **2009**, 307-340.
- 10. Reetz, M. T., Biocatalysis in organic chemistry and biotechnology: past, present, and future. *J Am Chem Soc* **2013**, *135* (34), 12480-12496.

- 11. O'Reilly, E.; Köhler, V.; Flitsch, S. L.; Turner, N. J., Cytochromes P450 as useful biocatalysts: addressing the limitations. *Chem Commun* **2011**, *47* (9), 2490-2501.
- 12. Pretzler, M.; Rompel, A., What causes the different functionality in type-III-copper enzymes? A state of the art perspective. *Inorg Chim A* **2018**, *481*, 25-31.
- 13. Palomo, J. M., Artificial enzymes with multiple active sites. *Curr Opinion Green Sus Chem* **2021**, *29*, 100452.
- 14. Su, J.; Wang, P.; Zhou, W.; Peydayesh, M.; Zhou, J.; Jin, T.; Donat, F.; Jin, C.; Xia, L.; Wang, K., Single-site iron-anchored amyloid hydrogels as catalytic platforms for alcohol detoxification. *Nature Nanotech* **2024**, *19*, 1168–1177.
- 15. Coelho, P. S.; Brustad, E. M.; Kannan, A.; Arnold, F. H., Olefin cyclopropanation via carbene transfer catalyzed by engineered cytochrome P450 enzymes. *Science* **2013**, *339* (6117), 307-310.
- 16. Zhao, L.-P.; Mai, B. K.; Cheng, L.; Gao, F.; Zhao, Y.; Guo, R.; Wu, H.; Zhang, Y.; Liu, P.; Yang, Y., Biocatalytic enantioselective C (sp 3)—H fluorination enabled by directed evolution of non-haem iron enzymes. *Nat Syn* **2024**, *3*, 967-975.
- 17. Zhou, Q.; Chin, M.; Fu, Y.; Liu, P.; Yang, Y., Stereodivergent atom-transfer radical cyclization by engineered cytochromes P450. *Science* **2021**, *374* (6575), 1612-1616.
- 18. Wang, Y.; Xue, P.; Cao, M.; Yu, T.; Lane, S. T.; Zhao, H., Directed evolution: methodologies and applications. *Chem Rev* **2021**, *121* (20), 12384-12444.
- 19. Mukherjee, S., Isolation and purification of industrial enzymes: advances in enzyme technology. In *Advances in Enzyme Technology*, Elsevier: **2019**; pp 41-70.
- 20. Page, C. G.; Cooper, S. J.; DeHovitz, J. S.; Oblinsky, D. G.; Biegasiewicz, K. F.; Antropow, A. H.; Armbrust, K. W.; Ellis, J. M.; Hamann, L. G.; Horn, E. J., Quaternary charge-transfer complex enables photoenzymatic intermolecular hydroalkylation of olefins. *J Am Chem Soc* **2020**, *143* (1), 97-102.
- 21. Davis, H. J.; Ward, T. R., Artificial metalloenzymes: challenges and opportunities. *ACS central Science* **2019**, *5* (7), 1120-1136.
- 22. Leone, L.; De Fenza, M.; Esposito, A.; Maglio, O.; Nastri, F.; Lombardi, A., Peptides and metal ions: A successful marriage for developing artificial metalloproteins. *J Peptide Sci* **2024**, *30*, e3606.
- 23. Wang, D.; Ingram, A. A.; Okumura, A.; Spaniol, T. P.; Schwaneberg, U.; Okuda, J., Benzylic C (sp3)—H Bond Oxidation with Ketone Selectivity by a Cobalt (IV)-Oxo Embedded in a β-Barrel Protein. *Chem Eur J* **2024**, *30* (5), e202303066.
- 24. McFadden, K. M.; Kays, L. G.; Boucher, D. G.; Minteer, S. D., Bioelectrocatalysis for Synthetic Applications: Utilities and Challenges. *Curr Opinion Electrochem* **2024**, *44*, 101458.
- 25. Boucher, D. G.; Carroll, E.; Nguyen, Z. A.; Jadhav, R. G.; Simoska, O.; Beaver, K.; Minteer, S. D., Bioelectrocatalytic Synthesis: Concepts and Applications. *Angew Chem* **2023**, *135* (46), e202307780.

- 26. García-Fernández, A.; Megens, R. P.; Villarino, L.; Roelfes, G., DNA-accelerated copper catalysis of Friedel–Crafts conjugate addition/enantioselective protonation reactions in water. *J. Am. Chem. Soc.* **2016,** *138* (50), 16308-16314.
- 27. Coquière, D.; Feringa, B. L.; Roelfes, G., DNA-based catalytic enantioselective Michael reactions in water. *Angew. Chem.*, *Int. Ed.* **2007**, *46* (48), 9308-9311.
- 28. Sandoval, B. A.; Hyster, T. K., Emerging strategies for expanding the toolbox of enzymes in biocatalysis. *Curr Opin Chem Biol* **2020**, *55*, 45-51.
- 29. Yu, K.; Zou, Z.; Igareta, N. V.; Tachibana, R.; Bechter, J.; Köhler, V.; Chen, D.; Ward, T. R., Artificial Metalloenzyme-Catalyzed Enantioselective Amidation via Nitrene Insertion in Unactivated C (sp 3)–H Bonds. *J Am Chem Soc* **2023**, *145* (30), 16621-16629.
- 30. Mukherjee, P.; Sairaman, A.; Deka, H. J.; Jain, S.; Mishra, S. K.; Roy, S.; Bhaumik, P.; Maiti, D., Enantiodivergent synthesis of isoindolones catalysed by a Rh (III)-based artificial metalloenzyme. *Nature Synthesis* **2024**, *3*, 835-845.
- 31. Natoli, S. N.; Hartwig, J. F., Noble—metal substitution in hemoproteins: an emerging strategy for abiological catalysis. *Acc Chem Res* **2019**, *52* (2), 326-335.
- 32. Yamamura, K.; Kaiser, E. T., Studies on the oxidase activity of copper (II) carboxypeptidase A. *Chem Comm* **1976**, (20), 830-831.
- 33. Mahammed, A.; Gray, H. B.; Weaver, J. J.; Sorasaenee, K.; Gross, Z., Amphiphilic corroles bind tightly to human serum albumin. *Biocon Chem* **2004**, *15* (4), 738-746.
- 34. Mahammed, A.; Gross, Z., Albumin-conjugated corrole metal complexes: extremely simple yet very efficient biomimetic oxidation systems. *J Am Chem Soc* **2005**, *127* (9), 2883-2887.
- 35. Albanese, D. C.; Gaggero, N., Albumin as a promiscuous biocatalyst in organic synthesis. *RSC Adv.* **2015,** *5* (14), 10588-10598.
- 36. Reetz, M. T.; Jiao, N., Copper–phthalocyanine conjugates of serum albumins as enantioselective catalysts in Diels–Alder reactions. *Angew. Chem. Int. Ed.* **2006**, *45* (15), 2416-2419.
- 37. Hena Jr, J. Y.; Kankanamage, R. N.; Wei, Z.; He, J.; Rusling, J. F., Chiral Biocatalytic Oxidations at 90° C in Microemulsions Driven by Electrocatalytic Oxygen Reduction to Hydrogen Peroxide. *ChemElectroChem* **2024**, e202300584.
- 38. Kumar, C. V.; Buranaprapuk, A., *Chiral Photochemical Scissors Targeting Proteins*. World Scientific: 2019.
- 39. Pasternack, R. F.; Gibbs, E. J.; Hoeflin, E.; Kosar, W. P.; Kubera, G.; Skowronek, C. A.; Wong, N. N.; Muller-Eberhard, U., Hemin binding to serum proteins and the catalysis of interprotein transfer. *Biochem* **1983**, *22* (8), 1753-1758.

- 40. Kundu, B. K.; Upadhyay, S. N.; Sinha, N.; Ganguly, R.; Grabchev, I.; Pakhira, S.; Mukhopadhyay, S., Pyrene-based fluorescent Ru (II)-arene complexes for significant biological applications: catalytic potential, DNA/protein binding, two photon cell imaging and in vitro cytotoxicity. *Dalton T* **2022**, *51* (10), 3937-3953.
- 41. Kumar, C. V.; Buranaprapuk, A., Tuning the selectivity of protein photocleavage: spectroscopic and photochemical studies. *J Am Chem Soc* **1999**, *121* (17), 4262-4270.
- 42. Kumar, C. V.; Buranaprapuk, A.; Sze, H. C.; Jockusch, S.; Turro, N. J., Chiral protein scissors: High enantiomeric selectivity for binding and its effect on protein photocleavage efficiency and specificity. *PNAS* **2002**, *99* (9), 5810-5815.
- 43. Duff Jr, M. R.; Kumar, C. V., Site-Selective Photocleavage of Proteins by Uranyl Ions. *Angew Chem In Ed* **2006**, *45* (1), 137-139.
- 44. Puglia, M. K.; Malhotra, M.; Chivukula, A.; Kumar, C. V., "Simple-Stir" Heterolayered MoS2/Graphene Nanosheets for Zn–Air Batteries. *ACS Appl Nano Mater* **2021**, *4* (10), 10389-10398.
- 45. Chen, Y.; Qu, S.; Song, Q.; Shi, W.; Li, H.; Yao, Q.; Chen, L., Synergistically optimized electrical and thermal transport properties in copper phthalocyanine-based organic small molecule with nanoscale phase separations. *ACS Appl Mater Interfaces* **2021**, *13* (13), 15064-15072.
- 46. Sasmal, M.; Bhowmick, R.; Musha Islam, A. S.; Bhuiya, S.; Das, S.; Ali, M., Domain-specific association of a phenanthrene–pyrene-based synthetic fluorescent probe with bovine serum albumin: Spectroscopic and molecular docking analysis. *ACS Omega* **2018**, *3* (6), 6293-6304.
- 47. Flores, M.; Olson, T. L.; Wang, D.; Edwardraja, S.; Shinde, S.; Williams, J. C.; Ghirlanda, G.; Allen, J. P., Copper environment in artificial metalloproteins probed by electron paramagnetic resonance
- spectroscopy. J. Phys. Chem. B 2015, 119 (43), 13825-13833.
- 48. Rusling, J. F., Green synthesis via electrolysis in microemulsions. *Pure Appl Chem* **2001**, *73* (12), 1895-1905.
- 49. Otto, K.; Hofstetter, K.; Röthlisberger, M.; Witholt, B.; Schmid, A., Biochemical characterization of StyAB from Pseudomonas sp. strain VLB120 as a two-component flavin-diffusible monooxygenase. *J Bacteriology* **2004**, *186* (16), 5292-5302.
- 50. Xiao, H.; Dong, S.; Liu, Y.; Pei, X.-Q.; Lin, H.; Wu, Z.-L., A new clade of styrene monooxygenases for (R)-selective epoxidation. *Catal. Sci. Technol.* **2021**, *11* (6), 2195-2201.
- 51. Savenkova, M. I.; Kuo, J. M.; Ortiz de Montellano, P. R., Improvement of peroxygenase activity by relocation of a catalytic histidine within the active site of horseradish peroxidase. *Biochemistry* **1998**, *37* (30), 10828-10836.

- 52. Heine, T.; Scholtissek, A.; Hofmann, S.; Koch, R.; Tischler, D., Accessing Enantiopure Epoxides and Sulfoxides: Related Flavin-Dependent Monooxygenases Provide Reversed Enantioselectivity. *ChemCatChem* **2020**, *12* (1), 199-209.
- 53. Cui, C.; Guo, C.; Lin, H.; Ding, Z.-Y.; Liu, Y.; Wu, Z.-L., Functional characterization of an (R)-selective styrene monooxygenase from streptomyces sp. NRRL S-31. *Enzyme and Microbial Technology* **2020,** *132*, 109391.
- 54. Nöthe, C.; Hartmans, S., Formation and degradation of styrene oxide stereoisomers by different microorganisms. *Biocatalysis* **1994,** *10* (1-4), 219-225.
- 55. Huang, W.-C.; Cullis, P. M.; Raven, E. L.; Roberts, G. C., Control of the stereo-selectivity of styreneepoxidation by cytochrome P450 BM3 using structure-based mutagenesis. *Metallomics* **2011**, *3* (4), 410-416.
- 56. Zhao, P.; Chen, J.; Ma, N.; Chen, J.; Qin, X.; Liu, C.; Yao, F.; Yao, L.; Jin, L.; Cong, Z., Enabling highly (R)-enantioselective epoxidation of styrene by engineering unique non-natural P450 peroxygenases. *Chem Sci* **2021**, *12* (18), 6307-6314.
- 57. Yan, Y.; Wu, J.; Hu, G.; Gao, C.; Guo, L.; Chen, X.; Liu, L.; Song, W., Current state and future perspectives of cytochrome P450 enzymes for C–H and C= C oxygenation. *Syn Sys Biotech* **2022**, *7* (3), 887-899.
- 58. Wang, L.; Wei, S.; Pan, X.; Liu, P.; Du, X.; Zhang, C.; Pu, L.; Wang, Q., Enhanced Turnover for the P450 119 Peroxygenase-Catalyzed Asymmetric Epoxidation of Styrenes by Random Mutagenesis. *Chem Eur J* **2018**, *24* (11), 2741-2749.
- 59. Albanese, D. C. M.; Gaggero, N., Albumin as a promiscuous biocatalyst in organic synthesis. *Rsc Adv* **2015,** *5* (14), 10588-10598.
- 60. Ozawa, T.; Hanaki, A., The first ESR spin-trapping evidence for the formation of hydroxyl radical from the reaction of copper (II) complex with hydrogen peroxide in aqueous solution. *Chem Comm* **1991**, , 330-332.
- 61. Allen, S. E.; Walvoord, R. R.; Padilla-Salinas, R.; Kozlowski, M. C., Aerobic copper-catalyzed organic reactions. *Chem Rev* **2013**, *113* (8), 6234-6458.
- 62. Yasufuku, Y.; Ueji, S.-i., Effect of temperature on lipase-catalyzed esterification in organic solvent. *Biotech Lett* **1995**, *17*, 1311-1316.
- 63. Takeda, K.; Wada, A.; Yamamoto, K.; Moriyama, Y.; Aoki, K., Conformational change of bovine serum albumin by heat treatment. *J Protein Chem* **1989**, *8*, 653-659.
- 64. Li, W.; Min, C.; Tan, F.; Li, Z.; Zhang, B.; Si, R.; Xu, M.; Liu, W.; Zhou, L.; Wei, Q., Bottom-up construction of active sites in a Cu–N4–C catalyst for highly efficient oxygen reduction reaction. *ACS Nano* **2019**, *13* (3), 3177-3187.

- 65. Jin, L.; Thanneeru, S.; Cintron, D.; He, J., Bioinspired Design of Hybrid Polymer Catalysts with Multicopper Sites for Oxygen Reduction. *ChemCatChem* **2020**, *12* (23), 5932-5937.
- 66. Liaqat, M.; Kankanamage, R. N. T.; Duan, H.; Shimogawa, R.; Sun, J.; Nielsen, M.; Shaaban, E.; Zhu, Y.; Gao, P.; Rusling, J. F., He, J. Single-Atom Cobalt Catalysts Coupled with Peroxidase Biocatalysis for C–H Bond Oxidation. *ACS Appl Mater Interfaces* **2023**, *15* (34), 40343-40354.

Table of Contents

